Velocity rotation curves in the equal mass and net null NUT charge gravimagnetic dipole spacetime

Clémentine Dassy[a] and Jan Govaerts[a,b,c]

[a] *Centre for Cosmology, Particle Physics and Phenomenology (CP3), Institut de Recherche en Mathématique et Physique (IRMP), Université catholique de Louvain (UCLouvain), 2, Chemin du Cyclotron, B-1348 Louvain-la-Neuve, Belgium*
E-mail: *Clementine.Dassy@uclouvain.be* (corresponding author), *Jan.Govaerts@uclouvain.be*
ORCID: http://orcid.org/0000-0002-0965-7848, http://orcid.org/0000-0002-8430-5180

[b] *International Chair in Mathematical Physics and Applications (ICMPA–UNESCO Chair) University of Abomey-Calavi, 072 B.P. 50, Cotonou, Republic of Benin*

[c] *Fellow of the Stellenbosch Institute for Advanced Study (STIAS), Stellenbosch, Republic of South Africa*

Abstract

The gravimagnetic dipole spacetime consists of two counter-rotating black holes of equal mass connected by a Misner string. For a particular distance in between them, the string is tensionless with the black holes at equilibrium with each other.

The geodesics of relativistic massive, or massless particles are considered, leading to the identification of circular rotation trajectories. The velocities of these trajectories are computed.

1 Introduction

General relativity admits a wide range of exact solutions, many of which display non-trivial structures even in the absence of matter. Among these, the gravimagnetic dipole spacetime, a recently described [1, 2, 3, 4] axisymmetric, asymptotically flat and stationary metric, consists of two counter-rotating NUT (Newman-Unti-Tamburino) black holes, of equal mass but opposite NUT charges, and connected by a Misner string. When the separation between the black holes is tuned precisely, the string becomes tensionless and the configuration is at equilibrium. By adimensionalising the system, the mass scale is removed and the gravimagnetic dipole spacetime is characterised by only one parameter, the NUT charge.

In this work, the motion of massive and massless test particles is studied in the equatorial plane, making full use of the available symmetries. Using a Hamiltonian formalism, an effective potential [5] is defined, leading to a condition for the existence of circular orbits. The rotation velocities associated with these orbits are then computed, thereby obtaining the velocity rotation curves for various values of the NUT parameter.

The recent study of the gravito-electromagnetic approximation to the gravimagnetic dipole [6] derived an approximate velocity rotation curve for circular orbits within the weak-field regime of the gravimagnetic dipole spacetime, identifying conditions under which a roughly flat rotation curve emerges without invoking dark matter. The present exact results are compared with these approximate analytic expressions, in the corresponding parameter range.

The term rotation curve is used here in a theoretical sense, to denote the velocity profile of test particles on a circular orbit. These curves serve more as a qualitative study of the spacetime geometry and the gravimagnetic influence of the NUT parameter, rather than as a direct counterpart of observed galaxy rotation curves. Nevertheless, given that the weak-field limit of this spacetime can yield approximately flat velocity profiles [6], qualitative analogies with dark-matter-motivated rotation curves may be noted, though no detailed observation comparison is attempted in the present work. Such a comparison would at the very least require a modelled inclusion of the contributions of ordinary and visible mass distributions in generic galaxies and their effect.

In the following, Section 2 reviews the gravimagnetic dipole metric. The conditions used to obtain a tensionless Misner string are described, allowing for the full characterisation of the spacetime with only one parameter, the NUT charge.

In Section 3, the Hamiltonian for massive and massless particles in this spacetime is presented and then used to define an effective potential for circular orbits. The number of circular orbits depends on the particle's energy and the value of the NUT parameter.

Section 4 finally presents the calculation of the velocity rotation curves along with the corresponding figures. Comparison is made with the results from [6], showing good agreement in the relevant domain of parameters.

2 The gravimagnetic dipole spacetime

Let us consider the gravimagnetic dipole spacetime metric. This configuration [1, 4] consists of the nonlinear superposition of two counter-rotating NUT objects [7] of equal masses $m > 0$ and opposite NUT charges $\pm\nu$ ($\nu \geq 0$), separated by a total distance $2k \geq 2m > 0$, and positioned symmetrically on the z-axis relative to $z = 0$.

In Weyl coordinates $(x^0, x^i) = (ct, \rho, \phi, z)$, the metric can be written as

$$ds^2 = -f(cdt - \omega d\phi)^2 + f^{-1}[e^{2\gamma}(d\rho^2 + dz^2) + \rho^2 d\phi^2]. \tag{2.1}$$

The functions f, ω and $e^{2\gamma}$ depend only on (ρ, z) and are written as follows:

$$f = \frac{|A|^2 - |B|^2}{|A+B|^2}, \quad e^{2\gamma} = \frac{|A|^2 - |B|^2}{64 d^4 \alpha_+^2 \alpha_-^2 R_+ R_- r_+ r_-}, \quad \omega = -4\frac{\Im[G(\bar{A}+\bar{B})]}{|A|^2 - |B|^2}, \tag{2.2}$$

given the following definitions (with $m \equiv Gm/c^2$, having the dimension of length in these units):

$$\begin{aligned} R_\pm(\rho, z) &= \sqrt{\rho^2 + (z \pm \alpha_+)^2}, & r_\pm(\rho, z) &= \sqrt{\rho^2 + (z \pm \alpha_-)^2}, \\ \alpha_\pm &= \sqrt{m^2 + k^2 - \nu^2 \pm 2d}, & d &= \sqrt{m^2 k^2 + \nu^2(k^2 - m^2)}. \end{aligned} \tag{2.3}$$

Finally, the functions A, B and G (which also depend only on (ρ, z)) are given by the following expressions:

$$\begin{aligned} A =& \frac{1}{2}\Big[(d-m^2)^2\alpha_+^2 + (d+m^2)^2\alpha_-^2\Big](R_+ - R_-)(r_+ - r_-) \\ &- \alpha_+\alpha_-\Big[2(d^2 - m^4)(R_+R_- + r_+r_-) + (d^2 + m^4)(R_+ + R_-)(r_+ + r_-)\Big] \\ &- 2imk\nu d\Big[(\alpha_+ - \alpha_-)(R_+r_+ - R_-r_-) - (\alpha_+ + \alpha_-)(R_+r_- - R_-r_+)\Big], \\ B =& -4d\Big\{(d-m^2)\alpha_-[m\alpha_+(R_+ + R_-) + ik\nu(R_+ - R_-)] \\ &\qquad + (d+m^2)\alpha_+[m\alpha_-(r_+ + r_-) + ik\nu(r_+ - r_-)]\Big\}, \\ G =& d\Big[-(d-m^2)^2\alpha_+ + (d+m^2)^2\alpha_- - 2ik\nu m^2(\alpha_+ - \alpha_-)\Big](R_+r_+ - R_-r_-) \\ &+ d\Big[(d-m^2)^2\alpha_+ + (d+m^2)^2\alpha_- + 2ik\nu m^2(\alpha_+ + \alpha_-)\Big](R_+r_- - R_-r_+) \\ &- m(d^2 + m^4)\alpha_+\alpha_-(R_+ + R_-)(r_+ + r_-) \\ &+ \frac{m}{2}\Big[(d-m^2)^2\alpha_+^2 + (d+m^2)^2\alpha_-^2 + 8ik\nu d^2\Big](R_+ - R_-)(r_+ - r_-) \\ &- 2m(d^2 - m^4)\alpha_+\alpha_-(R_+R_- + r_+r_-) \\ &- 2d(d-m^2)\alpha_-\Big[(\alpha_+ + 2m - z)(m\alpha_+ + ik\nu)R_+ - (\alpha_+ - 2m + z)(m\alpha_+ - ik\nu)R_-\Big] \\ &- 2d(d+m^2)\alpha_+\Big[(\alpha_- + 2m - z)(m\alpha_- + ik\nu)r_+ - (\alpha_- - 2m + z)(m\alpha_- - ik\nu)r_-\Big] \end{aligned} \tag{2.4, 2.5}$$

The functions f and $e^{2\gamma}$ are dimensionless; ω has a dimension of length, ensuring that every term in eq. (2.1) has proper dimensions.

For ease of use, here are the non-vanishing entries of the metric and its inverse:

$$\begin{aligned} &g_{tt} = -f, && g_{t\phi} = f\omega, && g_{\phi\phi} = \frac{\rho^2}{f} - f\omega^2, && g_{\rho\rho} = g_{zz} = f^{-1}e^{2\gamma}; \\ &g^{tt} = -f^{-1} + \frac{f\omega^2}{\rho^2}, && g^{t\phi} = \frac{f\omega}{\rho^2}, && g^{\phi\phi} = \frac{f}{\rho^2}, && g^{\rho\rho} = g^{zz} = fe^{-2\gamma}. \end{aligned} \tag{2.6}$$

This metric is asymptotically flat[1], with total mass $M = 2m$, a vanishing total NUT charge, and total angular momentum $J = 2k\nu$.

[1]Whilst the NUT solution[7] is not asymptotically flat with its Misner string then extending to infinity, the metric under investigation in this paper has a total NUT charge equal to zero (since the two superposed solutions have opposite NUT charges and equal masses) and is thus asymptotically flat. This situation is comparable to that of the Dirac string which extends to infinity for a single Dirac monopole, but is of finite extent when connecting two Dirac monopoles of opposite magnetic charges.

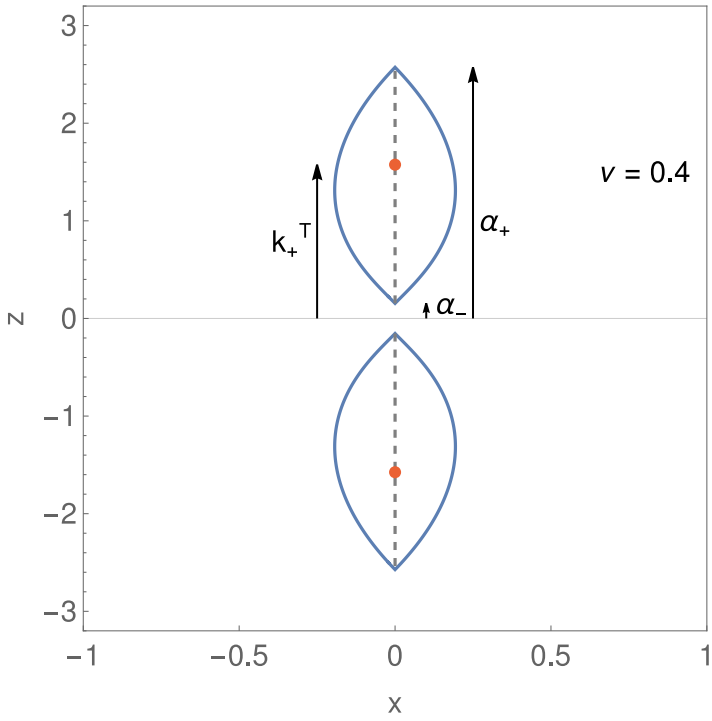

Figure 1: This graph shows a cut in the XZ plane of the spacetime. The plain blue lines represent the static limit and the orange dots the black holes. The dashed grey lines represent the horizons. Various quantities ($\alpha_\pm$, the limits of the horizons on the vertical axis) as well as the separation of the black holes $2k_+^T$ are also shown, for a gravimagnetic dipole spacetime with NUT parameter $\nu = 0.4$.

2.1 The values of m, k and ν

For $\nu = 0$, $\alpha_\pm = k \pm m$ and $d = km$ are real, and the metric, which is then static, describes a system of two non-rotating black holes each of mass m with a cosmic string of length $2(k - m)$. When $k = m$, the two black holes coalesce back into a single Schwarzschild one.

On the condition that $\alpha_\pm$ and d are real, the system defined by the gravimagnetic dipole spacetime with $\nu \neq 0$ consists of two black holes separated by a distance $2k$ and connected by a spinning cosmic string – called Misner string – of length $2\alpha_-$. These correspond to three sections of the z axis; the two black holes horizons for $\alpha_- < z < \alpha_+$ and $-\alpha_+ < z < -\alpha_-$, and the Misner string for $-\alpha_- < z < \alpha_-$. The masses of the black holes $M_{H_\pm}$ and their angular momenta, $J_{H_\pm}$ are functions of the three parameters m, k and ν [4].

The conditions for $\alpha_\pm$ and d to be real and non zero are given[4] by

$$k > k_+ \text{ or } k < k_-, \quad k_\pm(m, \nu) = \sqrt{m^2 + 2\nu^2} \pm |\nu| \,. \tag{2.7}$$

For the black holes to be at equilibrium with each other, the spinning cosmic string that joins them should be tensionless. The string tension per unit length $(1 - e^{-\gamma_S})/4$ is related to the value of the metric function at its center $e^{2\gamma_S} \equiv e^{2\gamma}(\rho = 0, z = 0)$.

This last conditions translates to

$$\left(\frac{\alpha_+ - \alpha_-}{2m}\right)^2 = 2 - \left(\frac{2m}{\alpha_+ + \alpha_-}\right)^2 . \tag{2.8}$$

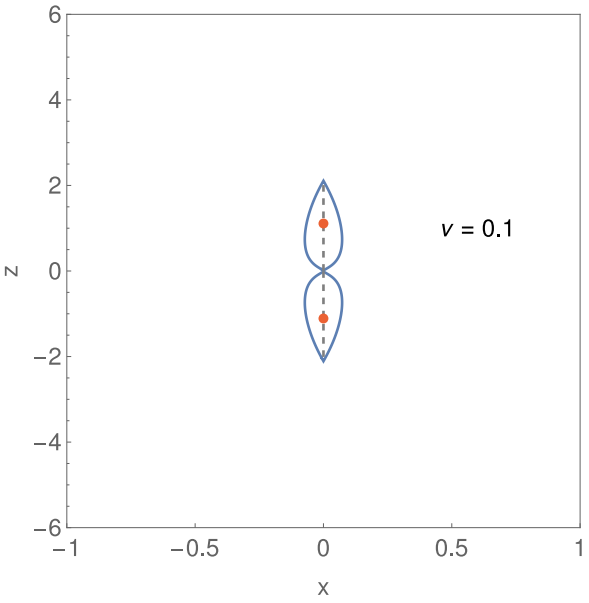

Figure 2: Cut of the spacetime along the XZ plane for $\nu = 0.1$. The orange dots represent the black holes. The blue lines represent the static limit. The dashed grey lines represent the horizon rods.

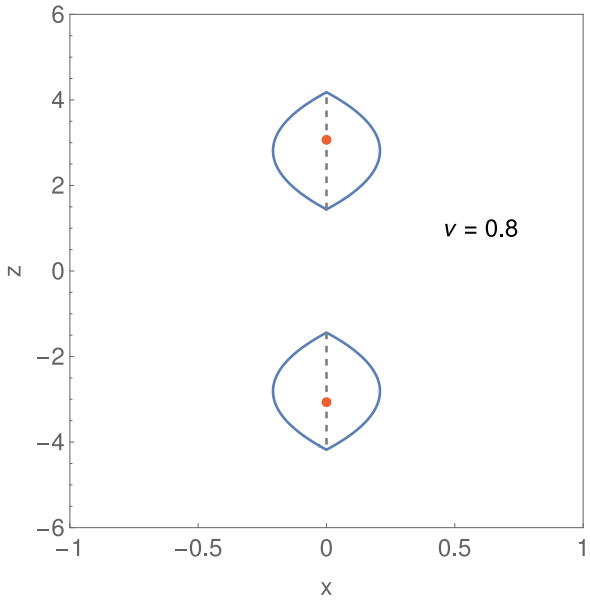

Figure 3: Cut of the spacetime along the XZ plane for $\nu = 0.8$. The orange dots represent the black holes. The blue lines represent the static limit. The dashed grey line represent the horizon rods.

This equation gives, as allowed values for k,

$$k(m,\nu) = \pm\sqrt{\frac{m\nu^6 + 3m^4\nu^2 \pm m^2\nu\sqrt{4vm^6 + 9m^4\nu^2 + 2m^2\nu^4 + \nu^6}}{m^4 - \nu^4}}. \tag{2.9}$$

Assembling eqs. (2.7) and (2.9) gives rise to a unique solution for k in the tensionless case:

$$k_+^T(m,\nu) = \sqrt{\frac{m\nu^6 + 3m^4\nu^2 + m^2\nu\sqrt{4m^6 + 9m^4\nu^2 + 2m^2\nu^4 + \nu^6}}{m^4 - \nu^4}}. \tag{2.10}$$

Lastly, for $k = m$, it was shown[1] that the system describes a Kerr black hole of mass $2m$ and Kerr parameter $a = \nu$, provided that $\nu < 2m$. In this case, $d = mk$, α_+ is real and α_- is imaginary, but α_- will not appear in any of the expressions of the metric, preserving its reality.

Since the system studied hereafter is the one corresponding to two rotating black holes at equilibrium at a fixed distance, the value $k = k_+^T$ will be used. The system is thus characterized by only two variables, ν and m.

Finally, when the parameters ν, k and m, as well as the coordinates ρ, ϕ, z and ct are divided by m, the metric is fully dimensionless. The symbols will be kept the same for readability's sake, but keep in mind now that every quantity is adimensional; only m will be replaced by 1.

2.2 Horizons and ergoregions

The static limits of the black holes ($g_{tt} = 0$) can be determined and plotted on a XZ slice of the space since it is axisymmetric. The general shape would be of two symmetric pears,

or two halves of a peanut shell, that grow further apart as ν increases. The separation of the black holes $2k$ diverges when $\nu \to 1$. The horizons are in the shape of rods, for $\rho = 0$, $-\alpha_+ < z < -\alpha_-$ and $\alpha_- < z < \alpha_+$. The two horizons touch only in the extreme case $\nu = 0$, at the singularity point of coordinates $\rho = 0 = z$, which will not be studied here.

Fig. 1 shows a cut in the XZ plane of the ergoregions and horizons, as well as the quantities $\alpha_\pm$ (the extremities of the horizons, as well as the intersection between the static limits and the vertical axis) and k (half the black holes separation) for a gravimagnetic dipole spacetime with NUT parameter $\nu = 0.4$.

Figs. 2 and 3 show the horizons and ergoregions for spacetimes with NUT parameters $\nu = 0.1$ and $\nu = 0.8$.

2.3 The metric functions in the equatorial plane

Before proceeding let us point out that at $z = 0$ the quantities in terms of which the metric components are defined now take the following values:

$$R = R_\pm(\rho, z = 0) = \sqrt{\rho^2 + \alpha_+^2}, \qquad r = r_\pm(\rho, z = 0) = \sqrt{\rho^2 + \alpha_-^2}, \tag{2.11}$$

allowing the following definitions

$$\begin{aligned}
A_0 &\equiv \frac{A(\rho, z=0)}{2\alpha_+\alpha_-} = -\Big[(d^2-1)(R^2+r^2) + (d^2+1)Rr\Big], \\
B_0 &\equiv \frac{B(\rho, z=0)}{2\alpha_+\alpha_-} = -2d\Big[(d-1)R + (d+1)r\Big], \\
G_0 &\equiv \frac{G(\rho, z=0)}{2\alpha_+\alpha_-} = G_r + iG_i, \\
G_i &\equiv \Im\left[\frac{G(\rho, z=0)}{2\alpha_+\alpha_-}\right] = -k\nu d\left[(d-1)R + (d+1)r\right], \\
G_r &\equiv \Re\left[\frac{G(\rho, z=0)}{2\alpha_+\alpha_-}\right] = -\left[((1+d)r + (-1+d)R)(-r + R + d(4 + r + R))\right].
\end{aligned} \tag{2.12}$$

With these redefinitions, it is ensured that A_0, B_0, and G_r and G_i are all real functions. They allow for the functions f, ω and $e^{2\gamma}$ to be written as

$$\begin{aligned}
f \equiv f(\rho, z=0) &= \frac{A_0 - B_0}{A_0 + B_0} = -\frac{8d}{(d-1)r + (d+1)R + 4d}, \\
\omega = \omega(\rho, z=0) &= \frac{-4G_i}{A_0 - B_0} = \frac{8dk\nu}{(1-d)r - (d+1)R + 4d}, \\
e^{2\gamma} = e^{2\gamma}(\rho, z=0) &= \frac{A_0^2 - B_0^2}{4d^4R^2r^2} = \frac{\left[(d+1)r + (d-1)R\right]^2\left[\{R(d+1) + r(d-1)\}^2 - 16d^2\right]}{16d^4r^2R^2}.
\end{aligned} \tag{2.13}$$

Every metric function is thus real for any value of $\rho \geq 0$ and $\nu \in]0, 1[$.

3 The effective potential for geodesics

Consider the general case of a free point particle — be it massive or massless — propagating in a spacetime whose geometry in coordinates (x^0, x^i) is characterised by the following metric and line element:

$$ds^2 = g_{\mu\nu}dx^\mu dx^\nu. \tag{3.1}$$

From the outset, herein the metric $g_{\mu\nu}$ is taken to be stationary (and asymptotically flat). Let us note that $x^0 = ct$ is the time coordinate with a dimension of length, and the x^i are spacelike (in general, curvilinear) coordinates of that same physical dimension.

As is well known[8, 9, 10], the particle's dynamics is derived from the Hamiltonian first-order action:

$$S[x^\mu, p_\mu; e] = \int du(\dot{x}^\mu p_\mu - H), \qquad H = \frac{1}{2}e(u)(g^{\mu\nu}p_\mu p_\nu + (\mu_0 c)^2), \tag{3.2}$$

with $u \in \mathbb{R}$ being an arbitrary worldline parametrisation (the dot standing for a derivative relative to u), μ_0 the mass of the particle ($\mu_0 > 0$ for a massive particle and $\mu_0 = 0$ for a massless one) and H the first-class Hamiltonian.

The conjugate momentum p_0 is constant due to the stationarity of the metric, and satisfies $p_0 = -E/c$, where E is the particle's energy. Additionally, when the metric is axisymmetric or spherically symmetric, p_ϕ is conserved and such that $p_\phi = L$ with L its (orbital) angular momentum. The positive definite einbein field $e(u)$ is playing the role of the Lagrange multiplier (and pure gauge degree of freedom) for the first-class constraint:

$$g^{\mu\nu}p_\mu p_\nu + (\mu_0 c)^2 = 0, \qquad c^2 g^{\mu\nu}p_\mu p_\nu + (\mu_0 c^2)^2 = 0. \tag{3.3}$$

The geodesic equations then read,

$$\frac{dx^\mu}{du} = e g^{\mu\nu}p_\nu, \qquad \frac{dp_\mu}{du} = -\frac{1}{2}e\frac{\partial g^{\rho\sigma}}{\partial x^\mu}p_\rho p_\sigma, \tag{3.4}$$

while being subjected as well to the first-class constraint eq. (3.3) to ensure invariance under orientation preserving worldline diffeomorphisms. Additionally, in the massive case the einbein is determined from the constraint as,

$$e = \pm\frac{1}{\mu_0 c}\sqrt{-g_{\mu\nu}\dot{x}^\mu\dot{x}^\nu}, \tag{3.5}$$

the upper sign corresponding to the standard square-root action for a relativistic massive particle, such that in a Minkowski spacetime solutions of positive energy propagate to the future.

3.1 The Hamiltonian equations of motion

Given the gravimagnetic dipole metric components, the general relation between coordinate time t and proper time τ is expressed as,

$$\frac{dt}{d\tau} = \frac{1}{\sqrt{-g_{tt}}} = \frac{1}{\sqrt{f}}, \qquad \frac{d\tau}{dt} = \sqrt{f}. \tag{3.6}$$

Furthermore, in Hamiltonian form, the geodesic equations of motion read as follows, for the spacetime coordinates,

$$c\frac{dt}{du} = e\left(g^{tt}p_t + g^{t\phi}p_\phi\right), \quad \frac{d\phi}{du} = e\left(g^{t\phi}p_t + g^{\phi\phi}p_\phi\right), \quad \frac{d\rho}{du} = e\,g^{\rho\rho}p_\rho, \quad \frac{dz}{du} = e\,g^{zz}p_z, \tag{3.7}$$

and for the conjugate momenta,

$$\frac{dp_t}{du} = 0, \qquad \frac{dp_\phi}{du} = 0, \qquad \frac{dp_\rho}{du} = -\frac{1}{2}e\frac{\partial g^{\mu\nu}}{\partial\rho}p_\mu p_\nu, \qquad \frac{dp_z}{du} = -\frac{1}{2}e\frac{\partial g^{\mu\nu}}{\partial z}p_\mu p_\nu, \tag{3.8}$$

subjected to the following constraint,

$$g^{tt}p_t^2 + 2g^{t\phi}p_t p_\phi + g^{\phi\phi}p_\phi^2 + g^{\rho\rho}p_\rho^2 + g^{zz}p_z^2 + (\mu_0 c)^2 = 0, \tag{3.9}$$

with the conserved conjugate momenta p_t and p_ϕ,

$$p_t = -\frac{E}{c}, \qquad p_\phi = L, \tag{3.10}$$

where E is the particle's relativistic energy and L its angular momentum (component along the axial symmetry axis), both taking constant and real values.

3.2 The effective potential

In the equatorial plane one has $p_z = 0 = z$ (see Appendix A for the verification of $dp_z/du = 0$, which is a non-trivial property) while the Hamiltonian of a massive ($\mu_0 > 0$) or massless ($\mu_0 = 0$) particle can be expressed as,

$$\mathcal{H} = \frac{e}{2}\frac{1}{c^2}\left(g^{tt}E^2 - 2g^{t\phi}E(cL) + g^{\phi\phi}(cL)^2 + g^{\rho\rho}p_\rho^2 + (\mu_0 c^2)^2\right). \tag{3.11}$$

This expression will now be used to define an effective potential to study circular orbits. From the definition of the conjugate momenta, p_ρ is expressed in terms of $d\rho/d\phi$ as

$$p_\rho = g_{\rho\rho}\frac{d\rho}{d\phi}\frac{d\phi}{du} = g_{\rho\rho}\left(g^{t\phi}p_t + g^{\phi\phi}p_\phi\right)\frac{d\rho}{d\phi}. \tag{3.12}$$

The constraint in eq. (3.9) can then be reexpressed as

$$\left(\frac{d\rho}{d\phi}\right)^2 + V(\rho, b) = 0, \tag{3.13}$$

where

$$V(\rho, b) = \frac{\rho^2}{e^{2\gamma}}\left[1 - \frac{\rho^2}{f^2}\frac{1}{(b-\omega)^2}\left(1 - f\left(\frac{\mu_0 c^2}{E}\right)^2\right)\right], \tag{3.14}$$

and $b = cL/E$ is the impact parameter[11].

Circular orbits correspond to the double condition that $V(\rho) = 0$ and $V'(\rho) = 0$ (a derivative relative to ρ is herein denoted with a prime, $'$). These equations are nontrivial but the first one can be used to define a critical impact parameter $b_\pm$, which allows to simplify the expression of the second one:

$$b_\pm = \omega \pm \frac{\rho}{f}\sqrt{1 - f\left(\frac{\mu_0 c^2}{E}\right)^2}, \qquad V(\rho, b = b_\pm) = 0. \tag{3.15}$$

The $\pm$ sign factor corresponds to the direction of rotation of the particle on its orbit, prograde or retrograde respectively. Again, this expression is valid for massive ($\mu_0 > 0$) or massless ($\mu_0 = 0$) particles.

The derivative of the potential with respect to ρ can be written as the sum of two terms:

$$V'(\rho, b)\Big|_{b=b_\pm} = \left(\frac{\rho^2}{e^{2\gamma}}\right)' \underbrace{\left[\ldots\right]}_{=0 \text{ for } b=b_\pm} + \frac{\rho^2}{e^{2\gamma}}\underbrace{\left[\ldots\right]'}_{=g(\rho)}. \tag{3.16}$$

The first is automatically zero by choice of $b = b_\pm$; the second term needs a bit more work. Since $e^{2\gamma} \neq 0$ for any value of (ν, ρ) such that $(\nu > 0, \rho > 0)$, the expression of interest will be only the large parenthesis that will be called $g(\rho)$ in the following.

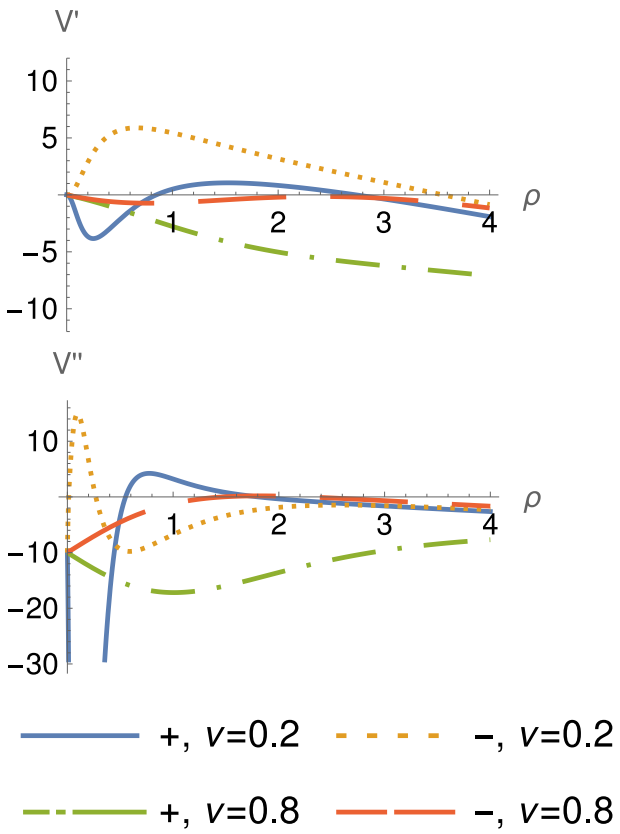

Figure 4: The top (resp. bottom) graph represents the first (resp. second) derivative of the potential as a function of ρ for massless particles, for two different rotation directions (prograde and retrograde) and two different values of ν. The number of possible circular orbits (from 0 to 4) depends on this parameter. The zeroes of the first derivative of the potential indicate the radii of the photon orbits, and the values of the second derivative at these radii indicate if the corresponding orbit is stable or unstable. For example, for $\nu = 0.2$ and a retrograde photon (orange dotted line), there is a unstable orbit at $\rho \approx 3.6$.

3.3 Massless particles

In the case of massless particles, $b_\pm = \omega \pm \frac{\rho}{f}$ and $\beta = 1$, and $g(\rho)$ in eq. (3.16) is given by the expression

$$g(\rho) = -\frac{2(\pm f^2\omega' + f - f'\rho)}{f\rho}. \tag{3.17}$$

The radii $\rho_\pm$ of the photon orbits are then given by the solutions of $g(\rho) = 0$, the sign factor corresponding to the one of $b_\pm$ and thus either a prograde or retrograde orbit. Depending on the values of the NUT parameter ν and of the energy E, eq. (3.17) will have between four and zero possible solutions. Then, according to the value of the the second derivative in ρ of the potential, V'', this orbit will be either stable ($V'' < 0$) or unstable ($V'' > 0$).

In Fig. 4, the top (resp. bottom) graph presents the first (resp. second) derivative of the potential for a massless particle as function of ρ and evaluated at $b = b_\pm$. For each graph, two values of the NUT parameter ($\nu = 0.2, \nu = 0.8$) are represented for the prograde and retrograde directions. The zeroes of the first derivative of the potential indicate the radii of the photon orbits, and the values of the second derivative at these radii indicate if the corresponding orbit is stable or unstable. For example, for $\nu = 0.2$

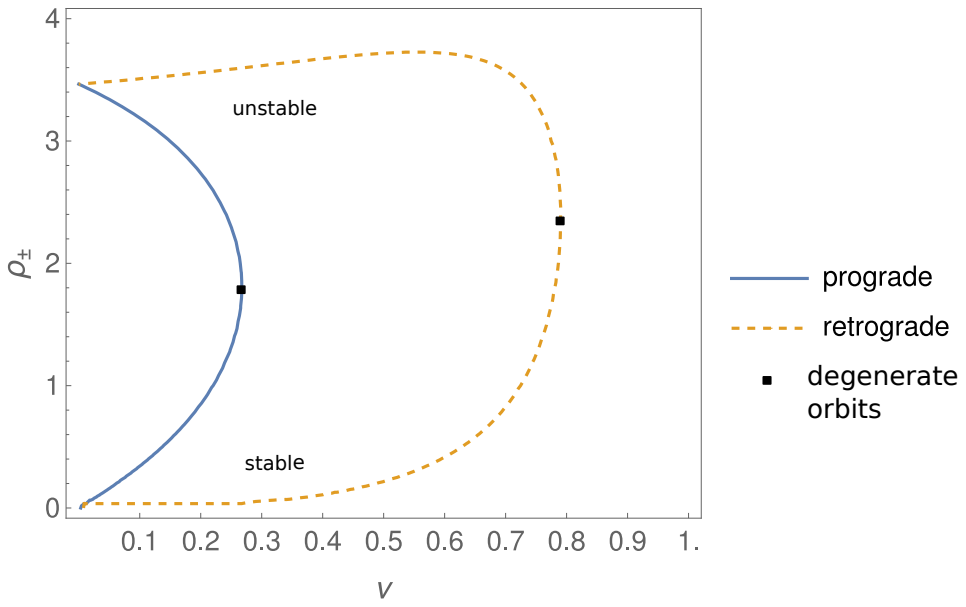

Figure 5: As functions of the parameter ν for massless particles, the radii of the possible circular orbits $\rho_\pm$ are represented. The plain line corresponds to prograde orbits, the dashed one to retrograde orbits. Depending on the value of ν, there will be between zero and four possible circular orbits. The black squares show the degenerate photon orbits, with the upper branches representing the unstable orbits, and the lower branches the stable orbits.

and a retrograde photon (orange dotted line), there is an unstable orbit at $\rho \approx 3.6$.

Eq. (3.17) can also be used to construct a bifurcation diagram, providing a visualisation of how the number of solutions varies with the value of ν. This is done in Fig. 5. As the value of ν grows, the number of photon orbits decreases. The prograde (resp. retrograde) orbits coalesce into one prograde (resp. retrograde) degenerate orbit (shown by a black square), then disappear. The coordinates of the saddle-node bifurcation can be numerically computed: for the prograde orbit, $\nu = 0.27, \rho = 1.78$, and for the retrograde orbit $\nu = 0.79, \rho = 2.30$.

The stability of the photon orbits can be determined from the general shape of V''; whenever photon orbits exist, the inner radius one will be stable, whilst the outer radius corresponding one will be retrograde. When there is only one orbit, the corresponding value of V'' is zero and it is degenerate.

3.4 Massive particules

Writing out the complete expression of $g(\rho)$ gives:

$$\begin{aligned} g(\rho) &= \frac{\rho\left[(b_\pm-\omega)(\rho f'(2E^2-c^4\mu_0^2 f)+2f(c^4\mu_0^2 f-E^2))+2\rho f\omega'(c^4\mu_0^2 f-E^2)\right]}{E^2 f^3 (b_\pm-\omega)^3} \\ &= \frac{2f^2(c^4\mu_0^2 \mp \beta E^2\omega') - f(c^4\mu_0^2\rho f'+2E^2)+2E^2\rho f'}{\beta^2 E^2 \rho f}, \\ &\text{with } \beta = \sqrt{1-f\left(\frac{\mu_0 c^2}{E}\right)^2},\ b_\pm = \omega \pm \frac{\rho}{f}\beta. \end{aligned} \tag{3.18}$$

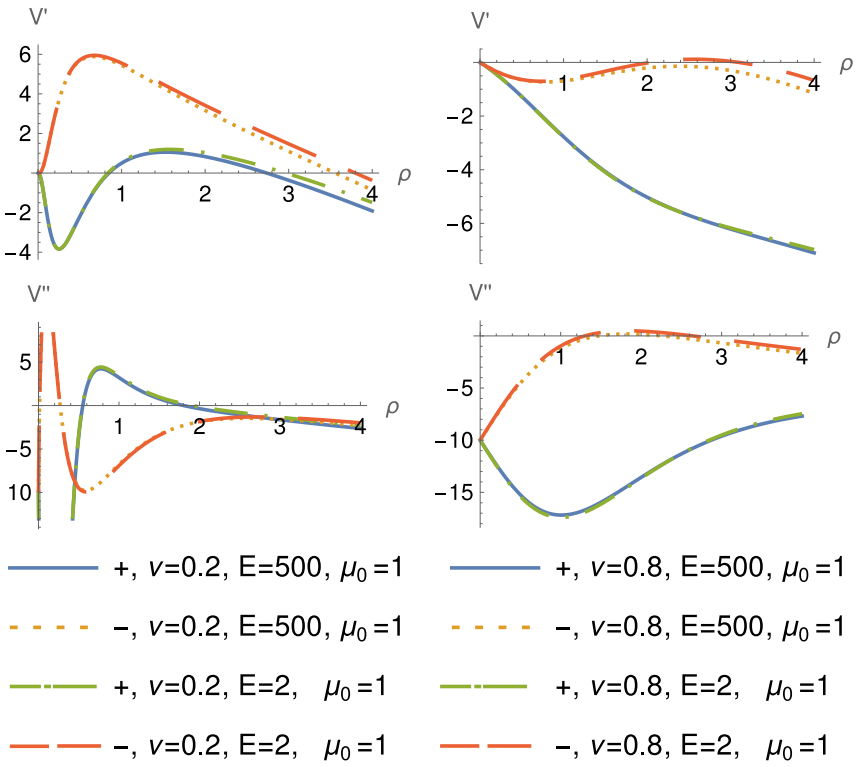

Figure 6: The left column has a NUT parameter $\nu = 0.2$ and the right column $\nu = 0.8$. The first (resp. second) row presents the first (resp. second) derivative V' (resp. V'') of the potential as functions of ρ and evaluated at $b = b_\pm$. Two values of the energy are represented ($E = 2$ and $E = 500$) for the prograde and retrograde directions. The zeroes of the first derivative of the potential indicate the radii at which circular orbits are possible, and the value of the second derivative at these radii indicate if the corresponding orbit is stable or unstable. For example, for $\nu = 0.2$, with an energy of $E = 2$ (green dashdotted line on the left column), there are two prograde orbits: one stable one at $\rho \approx 0.8$ and one unstable one at $\rho \approx 3$.

The radii $\rho_\pm$ of the circular orbits are then given by the solutions of $g(\rho) = 0$, the sign factor corresponding to the one of $b_\pm$ and thus either a prograde or retrograde orbit. According to the value of the the second derivative in ρ of the potential, V'', this orbit will be either stable ($V'' > 0$) or unstable ($V'' < 0$). Depending on the values of the NUT parameter ν and of the energy E, eq. (3.18) will have between four and zero possible solutions.

In Fig. 6, the left column has a NUT parameter $\nu = 0.2$ and the right column $\nu = 0.8$. The first (resp. second) row presents the first (resp. second) derivative of the potential, as function of ρ and evaluated at $b = b_\pm$. For each graph, two values of the energy are represented ($E = 2$ and $E = 500$) for the prograde and retrograde directions. The zeroes of the first derivative of the potential indicate the radii at which circular orbits are possible, and the value of the second derivative at these radii indicate if the corresponding orbit is stable or unstable. For example, for $\nu = 0.2$, with an energy of $E = 2$, (green dashdotted line on the left column) there are two prograde orbits: one stable one at $\rho \approx 0.8$ and one unstable one at $\rho \approx 3$.

The general shape of the second derivative of the potential allows for two remarks on the stability of the massive particle orbits. In general, when ν is small enough that there are photon orbits allowed, the massive particles orbiting "near" the photon orbits

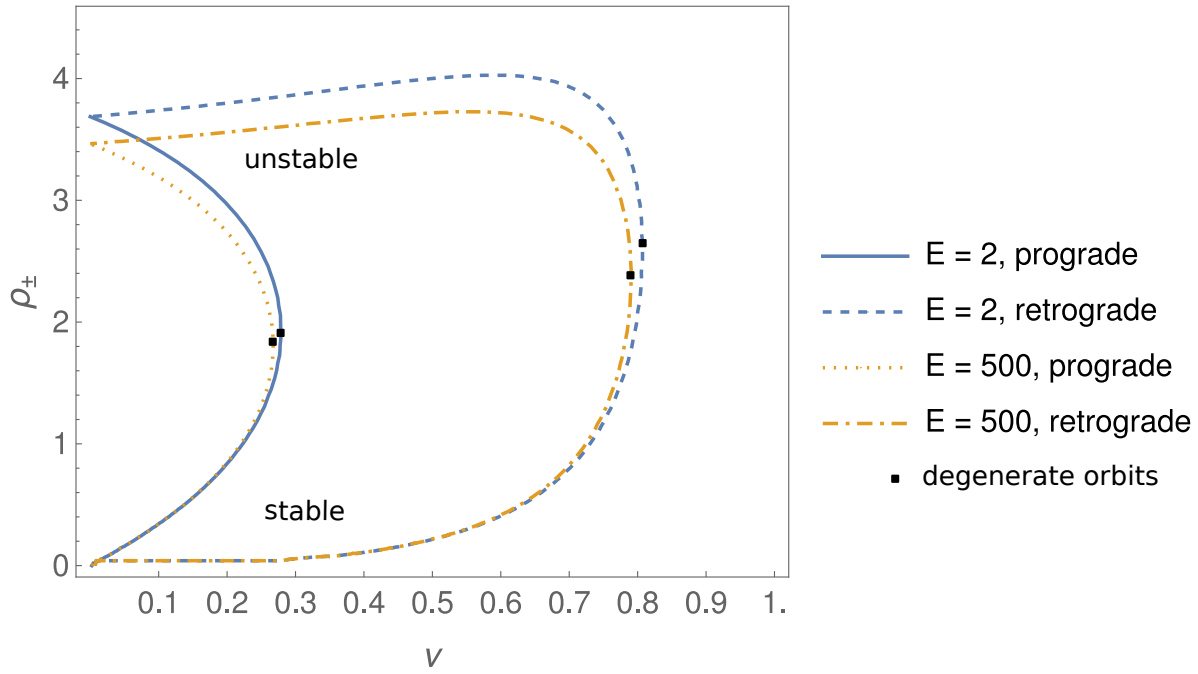

Figure 7: For different values of the energy E, as functions of the parameter ν, the radii of the possible circular orbits $\rho_\pm$ for massive particles. Depending on the value of the NUT parameter ν and the energy E, there is from 0 to 4 possible orbits. The value of the second derivative of the potential indicates the stability of the photon orbit. The degenerate orbits are shown as black squares.

(so with big values of the energy, $E \geq 1$) will have the same stability as the corresponding photon orbit. When the massive particles are orbiting with "big values" of ρ (general rule of thumb seems to be $\rho > 16$), the orbits will be stable.

In between, it is much more complicated to determine a general rule for the stability of the orbits; some more comments are made in Appendix B.

Eq. (3.18) can also be used to construct a bifurcation diagram, providing a visualisation of how the number of solutions (*i.e.* the number of possible circular orbits) varies with the value of ν. This is done in Fig. 7 for two different values of the energy. As the value of ν grows, the number of circular orbits decreases. The prograde (resp. retrograde) orbits coalesce into one prograde (resp. retrograde) orbit, then disappear. The previous remarks about stability can be visualised here: for $E = 2$ and $E = 500$, the upper branch of the prograde (and retrograde) orbits depict unstable orbits, whilst the lower branch depict stable orbits. The maximal value of ρ as a function of ν (*i.e.* the extremal points on the right of the curves, shown by a black square) depict the degenerate photon orbits.

4 Proper distance and velocity

The radar distance, or spatial distance[12] is the distance determined by the following procedure: an observer at point B sends a light signal to point A and receives its reflection back after some short interval of time. The radar distance between A and B is defined as half the total travel time (measured in the observer's proper time) multiplied by the speed of light.

This is expressed as

$$d\ell^2 = \left(g_{ij} - \frac{g_{0i}g_{0j}}{g_{00}} \right) dx^i dx^j. \tag{4.1}$$

This expression differs from the purely spatial distance by the term $\frac{-g_{0i}g_{0j}}{g_{00}} dx^i dx^j$, which takes into account the spatial deformation due to the advancement of time (note that it is also, of course, of the right dimension). It can be rewritten in the form:

$$d\ell^2 = \gamma_{ij} dx^i dx^j, \qquad \text{with} \qquad \gamma_{ij} = g_{ij} - \frac{g_{0i}g_{0j}}{g_{00}}. \tag{4.2}$$

The tensor γ_{ij} is the reciprocal of the contravariant spatial tensor g^{ij}. Indeed, from the relation $g^{\alpha\gamma} g_{\gamma\beta} = \delta^\alpha_\beta$, it follows that

$$g^{ij} g_{jk} + g^{i0} g_{0k} = \delta^i_k, \qquad g^{i0} = -\frac{g^{ij} g_{j0}}{g_{00}}, \tag{4.3}$$

and by inserting g^{i0} in the first of these two relations, one finds,

$$g^{ij} \gamma_{jk} = \delta^i_k. \tag{4.4}$$

Since in the general case $g_{\mu\nu}$ depends on x^0, it is meaningless to integrate $d\ell$ given a generic curved spacetime. The integral would be ill-defined since it would depend on the worldline, *i.e.*, the chosen path between the two points. Thus, generally speaking, in the context of generic curved spacetimes the concept of spatial distance remains valid at best only for infinitesimally small distances.

However, in the case of a stationary metric, $g_{\mu\nu}$ does not depend on x^0 and as such, the integral $\int d\ell$ is well-defined and can be used to determine the finite spatial distance between two simultaneous events.

Let us also note that in the axisymmetric spacetime under consideration here, the only cross term is $g_{t\phi}$ and there is no $g_{t\rho}$ crossterm. As such, the spatial radial distance corresponds to the proper distance $\bar{\rho}$ between ρ and ρ_0 defined as

$$\bar{\rho} = \int_{\rho_0}^{\rho} \sqrt{g_{\rho\rho}}\, d\rho. \tag{4.5}$$

Now that the concept of spatial distance is properly defined, the proper velocity (also known as celerity) can be defined as follows relative to the proper time along the worldline:

$$v_\tau^2 \equiv \gamma_{ij} \frac{dx^i}{d\tau} \frac{dx^j}{d\tau}, \tag{4.6}$$

as well as the velocity relative to the coordinate time, or coordinate velocity:

$$v_t^2 \equiv \gamma_{ij} \frac{dx^i}{dt} \frac{dx^j}{dt} = \left(\frac{d\tau}{dt} \right)^2 v_\tau^2, \qquad v_\tau^2 = \left(\frac{dt}{d\tau} \right)^2 v_t^2. \tag{4.7}$$

The coordinate velocity, denoted as $v_t > 0$ in the following, represents the particle's velocity as recorded by an asymptotic observer[2]. The proper velocity, $v_\tau > 0$, represents the ratio between the observer-measured displacement and the proper time elapsed on the clocks of the particle. In the following, focus is being put on the coordinate velocity as must be measured by an asymptotic observer, hence its physical relevance to this article.

[2]In view of the physical context, it is implicitly assumed herein that the stationary metric is asymptotically flat.

4.1 Proper distance in the gravimagnetic dipole spacetime

On the equatorial plane $z = 0$, the $g_{\rho\rho}$ factor can be written quite nicely:

$$\frac{e^{2\gamma}}{f} = \frac{|A+B|^2}{64\alpha_+^2\alpha_-^2 d^4 R^2 r^2}. \tag{4.8}$$

When divided by $\alpha_+\alpha_-$, at $z = 0$, $A + B$ is real and negative. As such,

$$\begin{aligned}\sqrt{g_{\rho\rho}} &= -\frac{A+B}{\alpha_+\alpha_-}\frac{1}{8d^2Rr} \\ &= \frac{1}{4}\left(1-\frac{1}{d^2}\right)\left(\frac{r}{R}+\frac{R}{r}\right)+\frac{1}{2d^2}+\frac{1}{d}\left(\frac{1}{R}-\frac{1}{r}\right)+\left(\frac{1}{R}+\frac{1}{r}\right)+\frac{1}{2}.\end{aligned} \tag{4.9}$$

This expression can be integrated in the following manner:

$$\begin{aligned}&\int \sqrt{g_{\rho\rho}}\,d\rho = \\ &\frac{-i(d^2-1)}{4d\alpha_+}\left\{\alpha_+^2 E\left(i\,\mathrm{arcsinh}\left(\frac{\rho}{\alpha_-}\right),\frac{\alpha_-^2}{\alpha_+^2}\right)+(\alpha_-^2-\alpha_+^2)F\left(i\,\mathrm{arcsinh}\left(\frac{\rho}{\alpha_-}\right),\frac{\alpha_-^2}{\alpha_+^2}\right)\right\} \\ &+\frac{1}{d^2}\left\{\frac{\rho}{2}\left(d^2+1\right)+d\left[(d-1)\log(\rho+r)+(d+1)\log(\rho+R)\right]\right\},\end{aligned} \tag{4.10}$$

where $F(\phi, m)$ and $E(\phi, m)$ are the elliptic integrals of the first and second kind defined as:

$$\begin{aligned}E(\phi,m) &= \int_0^\phi (1-m^2\sin^2\theta)^{1/2}\,d\theta, \\ F(\phi,m) &= \int_0^\phi (1-m^2\sin^2\theta)^{-1/2}\,d\theta.\end{aligned} \tag{4.11}$$

The proper radius between $\rho = 0$ and the position of a particle at coordinate ρ is then defined as

$$\bar{\rho} = \int_0^\rho \sqrt{g_{\rho\rho}}\,d\rho. \tag{4.12}$$

In Fig. 8, the proper radii for three different values of ν are plotted as function of ρ. It is not immediately obvious on the graph, but

$$\lim_{\rho\to\infty}\frac{\bar{\rho}(\rho)}{\rho} = 1. \tag{4.13}$$

Let us insist that $\bar{\rho}(\rho)$ depends not only on ρ, but also on the value of the NUT parameter ν.

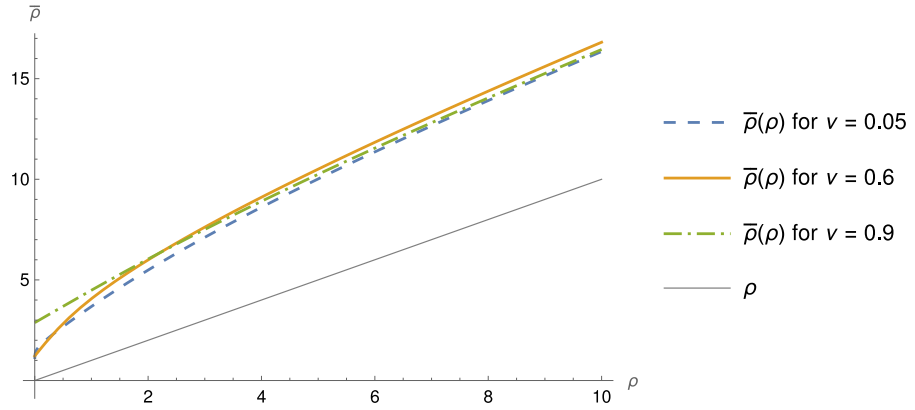

Figure 8: The proper radius for three values of the NUT parameter is plotted as a function of the coordinate radius. As a reference, the thin grey line is also the coordinate radius as a function of the coordinate radius, *i.e.* the identity.

4.2 Velocities for circular orbits in the gravimagnetic dipole spacetime

For a circular rotation curve in the equatorial plane, we require $d\rho/du = 0$ and $z = 0$, $dz/du = 0$, meaning that the velocity can be written from eqs. (3.7) and (4.7) as:

$$\begin{aligned} v_t^2 &= \left(g_{\phi\phi} - \frac{(g_{t\phi})^2}{g_{tt}}\right)\left(\frac{d\phi}{dt}\right)^2 \\ &= \left(g_{\phi\phi} - \frac{(g_{t\phi})^2}{g_{tt}}\right)\frac{g^{\phi\phi}b - g^{t\phi}}{g^{t\phi}b - g^{tt}} \\ \Rightarrow \frac{v_t^2}{c^2} &= \frac{\rho^2 f^3 (b-\omega)^2}{(\rho^2 + f^2\omega(b-\omega))^2}, \text{ where } b = b_\pm = \omega \pm \frac{\rho}{f}\sqrt{1 - f\left(\frac{\mu_0 c^2}{E}\right)^2}. \end{aligned} \tag{4.14}$$

The expressions of the potentials give a nice representation of where the circular orbits might be, but are not very practical in order to compute the velocities since one has to solve eq. (3.18) (numerically) to find the energy needed for a circular orbit for each value of the radius. Consequently, another approach is being used hereafter to determine the energy corresponding to a particular value of ρ.

4.3 The massive case

Replacing the value of $b_\pm$ obtained from eq. (3.18) in eq. (4.14), the velocity of a circular orbit as a function of the radius is given by

$$\frac{v_t^2}{c^2} = \frac{\beta^2\rho^2 f}{(\rho \pm \beta f\omega)^2}, \qquad \text{where } \beta = \sqrt{1 - f\left(\frac{\mu_0 c^2}{E}\right)^2}. \tag{4.15}$$

As was mentioned earlier, the value of the energy E in this last equation can be found for each value of ρ by solving eq. (3.18), but can also be expressed in a simpler manner.

One of the conditions for a circular orbit is $dp_\rho/du = 0$ and eq. (3.8) can be used to rewrite it as

$$\partial_\rho g^{tt} - 2\partial_\rho g^{t\phi}\frac{cL}{E} + \partial_\rho g^{\phi\phi}\left(\frac{cL}{E}\right)^2 = 0. \tag{4.16}$$

In conjunction with the constraint (3.9), this gives the expressions for the energy E and the angular momentum L for a circular orbit of radius ρ:

$$\begin{cases} E^2 = \dfrac{-(\mu_0 c^2)^2}{g^{tt} - 2g^{t\phi}b + g^{\phi\phi}b^2}, \\ (cL)^2 = \dfrac{-(\mu_0 c)^2 b^2}{g^{tt} - 2g^{t\phi}b + g^{\phi\phi}b^2}, \end{cases} \tag{4.17}$$

with

$$\frac{cL}{E} = b = \frac{\partial_\rho g^{t\phi} \pm \sqrt{(\partial_\rho g^{t\phi})^2 - \partial_\rho g^{\phi\phi}\partial_\rho g^{tt}}}{\partial_\rho g^{\phi\phi}}. \tag{4.18}$$

Fig. 9 shows the velocity of a massive particle on a circular orbit as a function of, on the leftmost (resp. rightmost) plot, the radius ρ (resp. the proper radius $\bar{\rho}$), for different values of the NUT parameter[3] ν. For the retrograde orbits, the opposite of the velocity is plotted for clarity's sake. Three of the curves (for the prograde and retrograde direction for $\nu = 0.05$ and for the retrograde direction for $\nu = 0.6$) have no real value for some interval of ρ (better seen on Fig. 10). This is due to the presence of photon orbits at these radii; the energy of a massive particle should be infinite, as can be seen in Fig. 11. In between the photon orbits, the energy of a massive particle on a circular orbit is imaginary (eq. (4.17)). This phenomenon does not occur for $\nu = 0.9$ since there are no photon orbits for this value of the NUT parameter. This is further displayed in Fig. 10, where the photon orbits are explicitly marked as grey lines: two prograde ($\rho_+^{0.05}$) and one retrograde ($\rho_-^{0.05}$, the other one goes to 0) photon orbits when $\nu = 0.05$ and two retrograde photon orbits for $\nu = 0.6$, $\rho_-^{0.06}$.

The squares on Fig. 9 show the degenerate orbits. For the prograde curve corresponding to $\nu = 0.05$, the orbits smaller than the inner photon orbit ($\rho < \rho_{+,i}^{0.05}$) depict stable orbits. For the prograde (respectively retrograde) curve with $\nu = 0.05$, the part between the corresponding outer photon orbits $\rho_{+,o}^{0.05}$ (resp. $\rho_{-,o}^{0.05}$) and the degenerate orbit (square) depict unstable orbits, and the part on the right of the degenerate orbit depicts stable orbits again. For $\nu = 0.6$, the prograde orbits are all stable, whilst the retrograde orbits are stable when smaller than the inner photon orbit ($\rho_{-,i}^{0.6}$), then stable between the outer photon orbit ($\rho_{-,o}^{0.6}$) and the degenerate orbit (square), then unstable again. For $\nu = 0.9$, the prograde orbits are all stable, and the retrograde orbits are stable between the two squares and unstable between them. This is further displayed in Fig. 10. The Newtonian velocity curve, $\rho^{-1/2}$, is also displayed on the left-most plot for comparison.

In Fig. 12 the velocity rotation curve, computed at $\nu = 0.999$, is compared with the approximate expression given in eq. (79) of [6]. In this regime ($\nu \approx 1$, tensionless Misner string), where the gravito-electromagnetic approximation is expected to hold, we find close agreement between the two results. (For $\nu = 0.999$ the following values are found: $k = 44.716$, $\alpha_+ = 46.107, \alpha_- = 43.279$.)

[3]For small ν, there are four allowed circular orbits on Fig. 7, but on Fig. 9, there are only two velocity rotation curves for $\nu = 0.6$, consisting of the merged stable and unstable parts of the curve. This is further detailed in Appendix B.

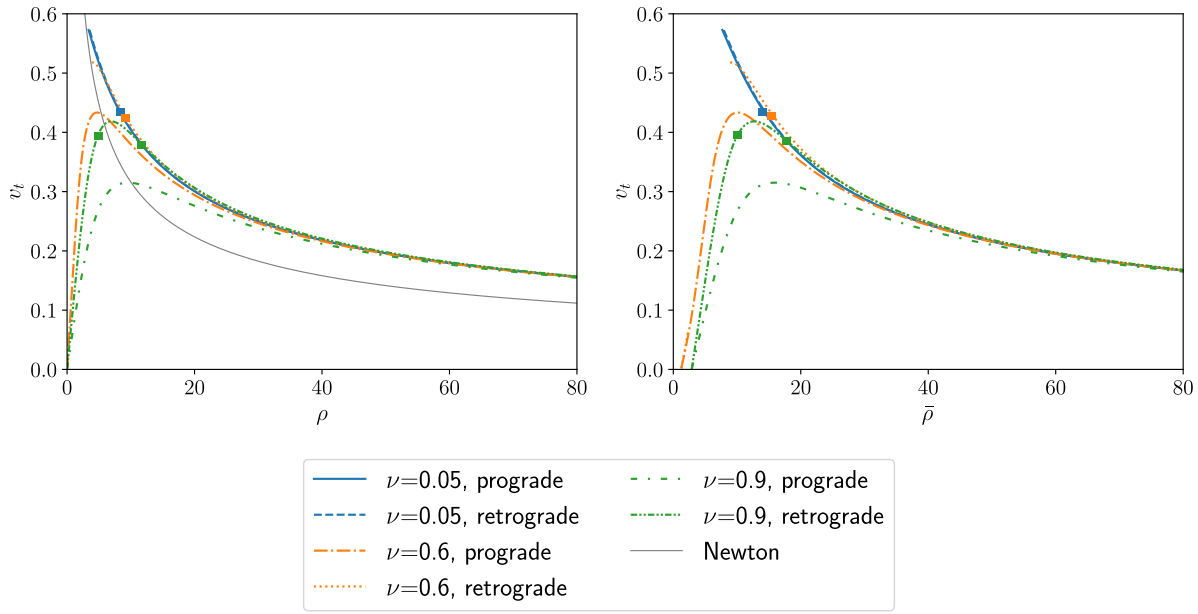

Figure 9: The velocity of a massive particle on a circular orbit is plotted as a function of, on the left-most (resp. right-most) plot, the radius ρ (resp. the proper radius $\bar{\rho}$), for different values of the NUT parameter ν. For the retrograde orbits, the opposite of the velocity is plotted for clarity's sake. Three of the curves (for the prograde and retrograde direction for $\nu = 0.05$ and for the retrograde direction for $\nu = 0.6$) are interrupted around $\rho \approx 5$ and under; there are no real velocities for a circular orbit of a massive particle. This is due to the presence of photon orbits at these radii; the energy of a massive particle should be infinite, as can be seen in Fig. 11. In between the photon orbits, the energy of a massive particle on a circular orbit should be imaginary. This phenomenon does not occur for $\nu = 0.9$ since there are no photon orbits for this value of the NUT parameter. The squares depict degenerate orbits. For the two curves corresponding to $\nu = 0.05$, prograde and retrograde, the leftmost parts of the curves ($\rho < 0.2$, better seen on Fig. 10) depict stable orbits, the part between $\rho \approx 3$ and the square depict unstable orbits, and the part on the right of the square depict stable orbits again. For $\nu = 0.6$, the prograde orbits are all stable, whilst the retrograde orbits are stable when smaller than the inner photon orbit, then stable between the outer photon orbit and the square, then unstable again. For $\nu = 0.9$, the prograde orbits are all stable, and the stable orbits are stable between the two squares and unstable between them. This is further displayed in Fig. 10. The Newtonian velocity curve, $\rho^{-1/2}$, is also displayed on the left-most plot for comparison.

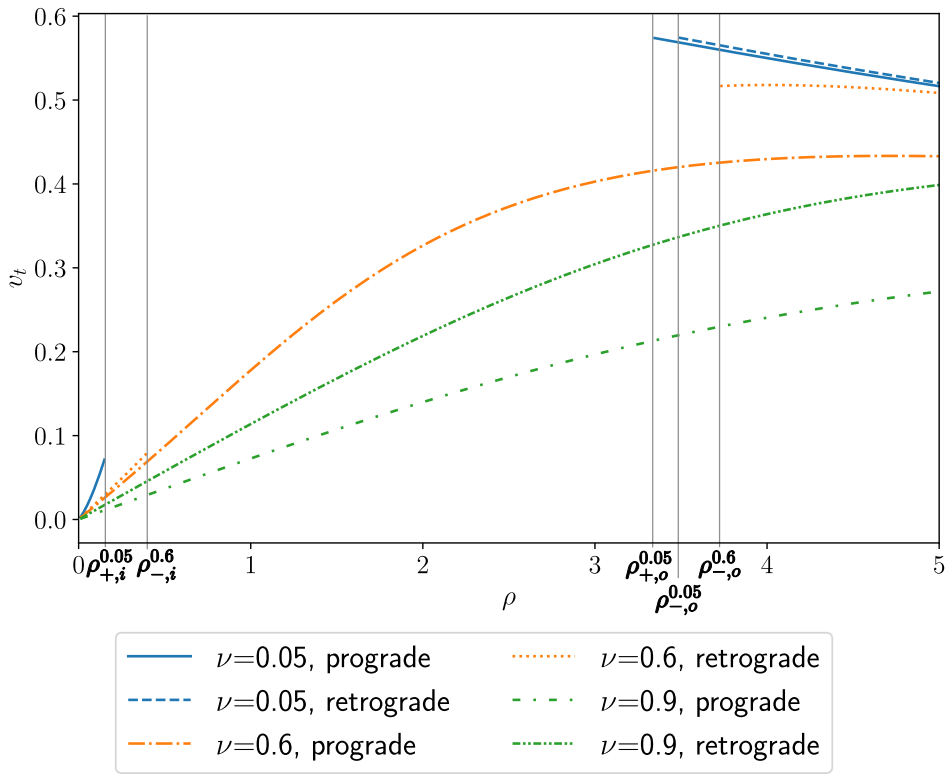

Figure 10: Zoom of the left panel of Fig. 9. The photon orbits are indicated where relevant: two prograde (inner $\rho^{0.05}_{+,i}$, outer $\rho^{0.05}_{+,o}$) and one retrograde (outer $\rho^{0.05}_{-,o}$, the inner radius goes to 0) photon orbits when $\nu = 0.05$ and two retrograde photon orbits for $\nu = 0.6$, (inner $\rho^{0.06}_{-,i}$ and outer $\rho^{0.06}_{-,o}$). Outside of the interval on ρ defined by these orbits, massive particles can orbit in the corresponding direction. In the intervals, no circular orbits are possible for massive particles. For the values of ρ depiced on this graph: for the two curves corresponding to $\nu = 0.05$, prograde and retrograde, the orbits smaller than the inner photon orbit are stable, and the orbits bigger than the outer photon orbits are unstable. For $\nu = 0.6$, the prograde orbits are all stable, whilst the retrograde orbits are stable when smaller than the inner photon orbit and stable when bigger than the outer photon orbit. For $\nu = 0.9$, every orbit depicted here is stable.

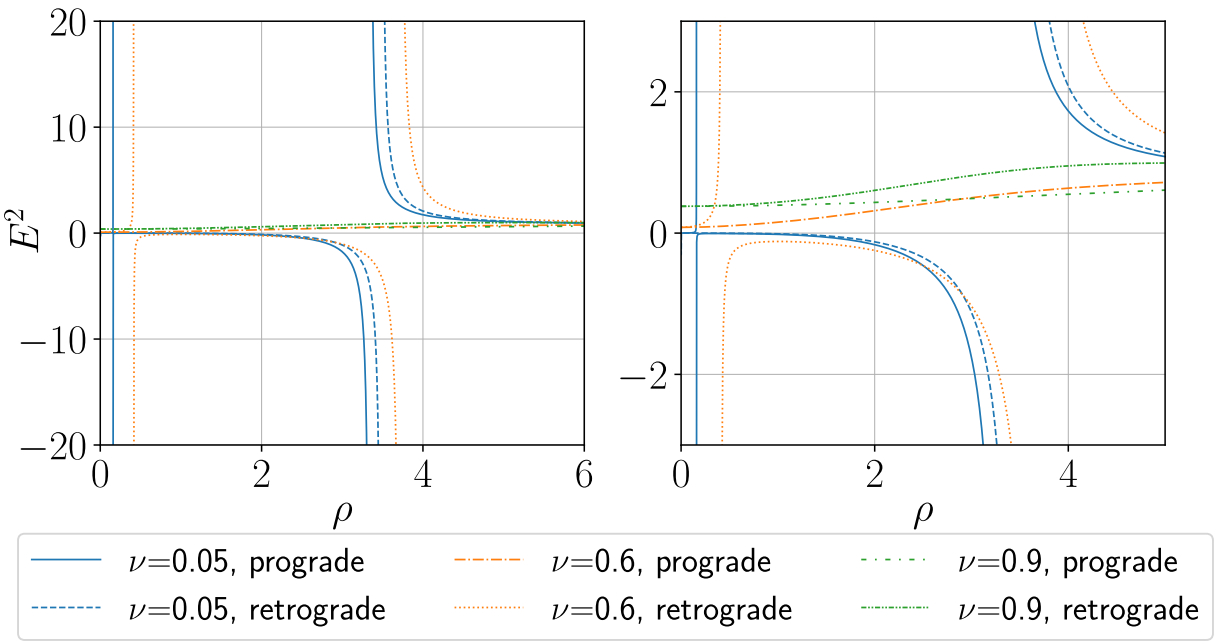

Figure 11: The squared value of the energy (eq. (4.17), with $\mu_0 = 1 = c$) is plotted as a function of the radius ρ for (prograde or retrograde) circular orbits and for different values of the NUT parameter. The right panel is the zoomed version of the left panel. The asymptotes towards positive infinity mark the radii at which photon orbits are permitted. In between, the energy is imaginary and there are no circular orbits. As $\rho \to \infty$, the energies go to 1, as is expected from our choice of $\mu_0 = 1 = c$.

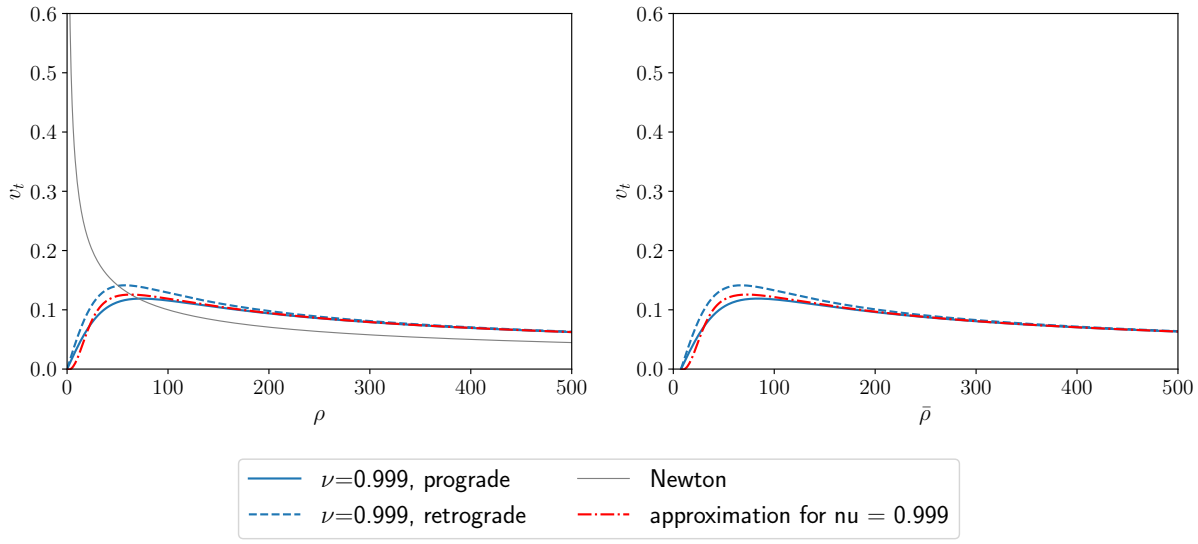

Figure 12: For a value of the NUT parameter of $\nu = 0.999$, the blue plain (resp. dashed) line depicts the exact velocity of a massive particle on a prograde (resp. retrograde) circular orbit. The red dashdotted line depicts the gravito-electromagnetic approximation in eq. (79) of Ref. [6].

4.4 The massless case

In the massless case, the value of the radius of a photon orbit for some value of the NUT parameter is given by the solution of eq. (3.17). Replacing $b_\pm = \omega \pm \frac{\rho}{f}$ in eq. (4.14), the velocity of the photons on their circular orbit is given by

$$\frac{v_{t,\pm}^2}{c^2} = \frac{\rho^2 f}{(\rho \pm f\omega)^2}, \tag{4.19}$$

where all functions are evaluated at $\rho = \rho_\pm$.

This velocity is plotted as a function of the NUT parameter ν on Fig. 13. As should be expected, the figure has again the shape of a bifurcation diagram. When the prograde (resp. retrograde) orbits coalesce together, the corresponding velocities also coalesce together.

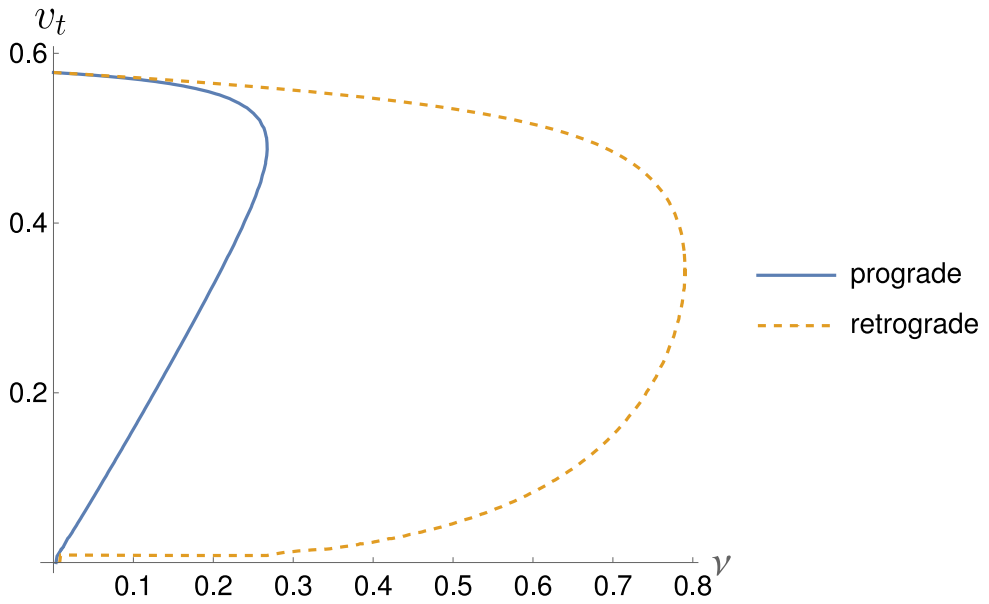

Figure 13: As functions of the NUT parameter ν, the velocities v_t for massless particles on circular orbits. The plain line corresponds to the prograde velocities, the dashed line to the opposite of the retrograde velocity.

5 Conclusion

This paper has presented a general method to compute the velocity of a massive, or massless, particle on a circular orbit in the equatorial plane of an axisymmetric stationary and asymptotically flat metric. The approach has then been applied specifically to the gravimagnetic dipole metric, allowing for an analysis of circular rotation curves for both massive and massless particles.

The next natural step would be to investigate the behaviour of particles not confined strictly to the equatorial plane. For example, if particles start in the neighbourhood of the equatorial plane but not in it, they should manifest an oscillatory behaviour around it. This phenomenon could be explored through perturbative methods.

Furthermore, the model could be enriched by adding matter distributions, superposed on the gravimagnetic dipole metric. Such modifications would allow for a more realistic

representation of astrophysical scenarios and would very likely influence the shape of the rotation curves.

A Condition in z is verified $\forall p_t, p_\phi$ in $z = 0$

The following equation should be trivially satisfied in $z = 0$ for any p_t and p_ϕ:

$$\begin{aligned} \frac{dp_z}{du} &= -\frac{1}{2} e \frac{\partial g^{\mu\nu}}{\partial z} p_\mu p_\nu \\ 0 &= \partial_z g^{tt} p_t^2 + 2\partial_z g^{t\phi} p_t p_\phi + \partial_z g^{\phi\phi}, \end{aligned} \tag{A.1}$$

and here are the derivatives in z of the metric:

$$\begin{cases} \partial_z g^{tt} = f^{-2}\partial_z f + \dfrac{1}{\rho^2}\left(\omega^2 \partial_z f + 2f\omega\partial_z\omega\right), \\ \partial_z g^{t\phi} = \dfrac{1}{\rho^2}\left(\omega^2 \partial_z f + 2f\omega\partial_z\omega\right), \\ \partial_z g^{\phi\phi} = \dfrac{1}{\rho^2}\partial_z f. \end{cases} \tag{A.2}$$

For eq. (A.1) to be verified $\forall \rho > 0, z = 0$, using (A.2), we need only to verify that for $\rho > 0, z = 0$, $\partial_z f = 0$ and $\partial_z \omega = 0$.

Let us start by noticing the following relations when $z = 0$:

$$\begin{aligned} R_\pm(\rho, z) &= \sqrt{\rho^2 + (z \pm \alpha_+)^2} \quad &\Rightarrow R_\pm|_{z=0} &= \sqrt{\rho^2 + \alpha_+^2} \equiv R, \\ r_\pm(\rho, z) &= \sqrt{\rho^2 + (z \pm \alpha_-)^2} \quad &\Rightarrow r_\pm|_{z=0} &= \sqrt{\rho^2 + \alpha_-^2} \equiv r, \\ \partial_z R_\pm(\rho, z) &= \frac{z \pm \alpha_+}{R_\pm(\rho, z)} \quad &\Rightarrow \partial_z R_\pm|_{z=0} &= \frac{\pm\alpha_+}{R}, \\ \partial_z r_\pm(\rho, z) &= \frac{z \pm \alpha_-}{r_\pm(\rho, z)} \quad &\Rightarrow \partial_z r_\pm|_{z=0} &= \frac{\pm\alpha_-}{r}. \end{aligned} \tag{A.3}$$

Let us first take a look at A and its derivative in z at $z = 0$:

$$\left.\frac{A(\rho, z)}{\alpha_+\alpha_-}\right|_{z=0} \equiv A_0 \in \mathbb{R}, \qquad \left.\partial_z \frac{A(\rho, z)}{\alpha_+\alpha_-}\right|_{z=0} \equiv \partial_z A_0 \in \mathbb{I}. \tag{A.4}$$

Similarly, for B,

$$\left.\frac{B(\rho, z)}{\alpha_+\alpha_-}\right|_{z=0} \equiv B_0 \in \mathbb{R}, \qquad \left.\partial_z \frac{B(\rho, z)}{\alpha_+\alpha_-}\right|_{z=0} \equiv \partial_z B_0 \in \mathbb{I}. \tag{A.5}$$

Thus we can write the following equalities:

$$\begin{aligned} \bar{A}_0 &= A_0, \qquad & \overline{(\partial_z A_0)} &= -\partial_z A_0, \\ \bar{A}_0 &= B_0, \qquad & \overline{(\partial_z B_0)} &= -\partial_z B_0. \end{aligned} \tag{A.6}$$

Let us now look at the expression for f and its derivative in z:

$$f = \frac{|A|^2 - |B|^2}{|A + B|^2} = \frac{A\overline{A} - B\overline{B}}{(A + B)\overline{(A + B)}}. \tag{A.7}$$

Its derivative in z, with $\partial_z A \equiv A'$ and $\partial_z B \equiv B'$ is thus given by:

$$\partial_z f = \frac{1}{(A+B)^2(\overline{A}+\overline{B})^2}\Big\{(A'\overline{A}+A\overline{A}'-B'\overline{B}-B\overline{B}')(A+B)(\overline{A}+\overline{B}) \\ -(A\overline{A}-B\overline{B})\Big((A'+B')(\overline{A}+\overline{B})+(A+B)(\overline{A}'+\overline{B}')\Big)\Big\}. \tag{A.8}$$

When $z=0$, using (A.6), this simplifies to

$$\partial_z f|_{z=0} = \left(\frac{1}{(A+B)^2(A+B)^2}\Big\{(A'A-AA'-B'B+BB')(A+B)(A+B) \\ -(AA-BB)\left((A'+B')(A+B)-(A+B)(A'+B')\right)\Big\}\right)_{z=0} \\ =0. \tag{A.9}$$

For G, the situation is a bit more complex, because both the imaginary and the real parts survive when $z=0$. We will then denote G as $G \equiv G_r + iG_i$.

We can then compute what happens to G and its derivative when $z=0$.

$$\frac{G}{\alpha_+\alpha_-}\bigg|_{z=0} \equiv G_r + iG_i, \qquad \partial_z \frac{G}{\alpha_+\alpha_-}\bigg|_{z=0} \equiv \partial_z G_r + i\partial G_i, \tag{A.10}$$

and in terms of these notations, it follows that:

$$\bar{G}_0 = G_r - iG_i, \qquad \overline{(\partial_z G_0)} = \partial_z G_r - i\partial_z G_i. \tag{A.11}$$

We can now finally compute ω and its derivative in z. We know that the expression for ω is given by:

$$\omega(\rho,z) = -4\frac{\Im(G(\overline{A}+\overline{B}))}{|A|^2-|B|^2}, \tag{A.12}$$

thus its derivative in z should look like:

$$\partial_z\omega(\rho,z) = \frac{-4}{(|A|^2-|B|^2)^2}\times\Big\{-4\Im\left\{G'(\overline{A}+\overline{B})+G(\overline{A}'+\overline{B}')\right\}\left\{|A|^2-|B|^2\right\} \\ +4\Im\left\{G(\overline{A}+\overline{B})\right\}(A'\overline{A}+A\overline{A}'-B'\overline{B}-B\overline{B}')\Big\}. \tag{A.13}$$

We now put $z=0$ and use (A.4) and (A.5) to reduce the expression to:

$$\partial_z\omega_0 = \frac{-4}{(|A_0|^2-|B_0|^2)^2}\times\Big\{-4\Im\left\{G_0'(A_0+B_0)-G_0(A_0'+B_0')\right\}\left\{|A_0|^2-|B_0|^2\right\} \\ +4\Im\left\{G_0(A_0+B_0)\right\}(A_0'A_0-A_0A_0'-B_0'B_0+B_0B_0')\Big\}. \tag{A.14}$$

The second line vanishes, and we now just have to verify that

$$Q \equiv \Im\left\{G_0'(A_0+B_0)-G_0(A_0'+B_0')\right\} = 0. \tag{A.15}$$

To do that, let us use (A.10), we get

$$Q = \Im\left\{(G'_r + iG'_i)(A_0 + B_0) - (G_r + iG_i)(A'_0 + B'_0)\right\}. \tag{A.16}$$

Since we know that $A_0, B_0 \in \mathbb{R}$ and $A'_0, B'_0 \in \mathbb{I}$,

$$Q = G'_i(A_0 + B_0) - G_r(A'_0 + B'_0), \tag{A.17}$$

which we will have to brute force our way through.

The easiest way is to realise that

$$\frac{G'_i}{A'_0 + B'_0} = m, \tag{A.18}$$

then divide (A.17) by $(A'_0+B'_0)$ and show that $m(A_0+B_0)-G_r = 0$ by looking individually at the factors for R^2, r^2, Rr, R and r, which are all 0. Also, there is no independent term.

Thus we find that $Q = 0$, which means that $\partial_z\omega_0 = 0$ and the derivatives in (A.2) are all identically 0, which verifies the equation (A.1) trivially for all $\rho > 0, z = 0$.

B There are at most two velocity rotation curves for any value of ν

For each value of ν, Fig. 9, 10, 12 show only two velocity rotation curves, whilst there are, for example for small values of ν, more than two possible circular orbits, as can be seen on Fig. 7. Fig. 14 shows the superposition of the bifurcation diagrams of the circular orbits of photons and of massive particles with different energies. The red line depicts a particular value of ν, that will be used in the following example to understand how the velocity rotation curves are constructed and the stability of the orbits determined.

Looking at eq. (4.17), there are two values of the energy squared for each value of ρ; one corresponds to the prograde orbit (with $b = b_+$) and one to the retrograde orbit (with $b = b_-$). Let us look only a the prograde orbit for now. There are then two values of the energy possible ($\pm\sqrt{E^2}$). So there is only one physical value of the energy for a prograde orbit.

Looking at it the other way around, for every value of the energy, there are at most two prograde circular orbits radii allowed, with these radii not corresponding to any other value of the energy.

On the bifurcation diagram in Fig. 14, this translates to the red line, representing the fact that $\nu = 0.6$, intersecting at most *twice* each continuous curve (prograde energies). Each of these intersections can be parametrised by the values (ν, ρ, E) and has one velocity associated to it, given by eq. (4.15).

For the particular value of $\nu = 0.6$, there is no prograde photon orbit, so the part of the velocity rotation curve on Fig. 10 corresponding to the intersection of the red line with the lower branches of the energies will "merge" with the part corresponding to the top branches, both these parts are stable.

This can be seen on Fig. 15; the orange dashdotted curve depicts the second derivative of the potential and is always positive ; thus the orbits are all stable.

Looking now at retrograde orbits on Fig. 14, there will be a discontinuity in the velocity rotation curve because no massive particles can have circular orbits on the radii between the photon orbits, here represented by the intersections of the red line with the thick black

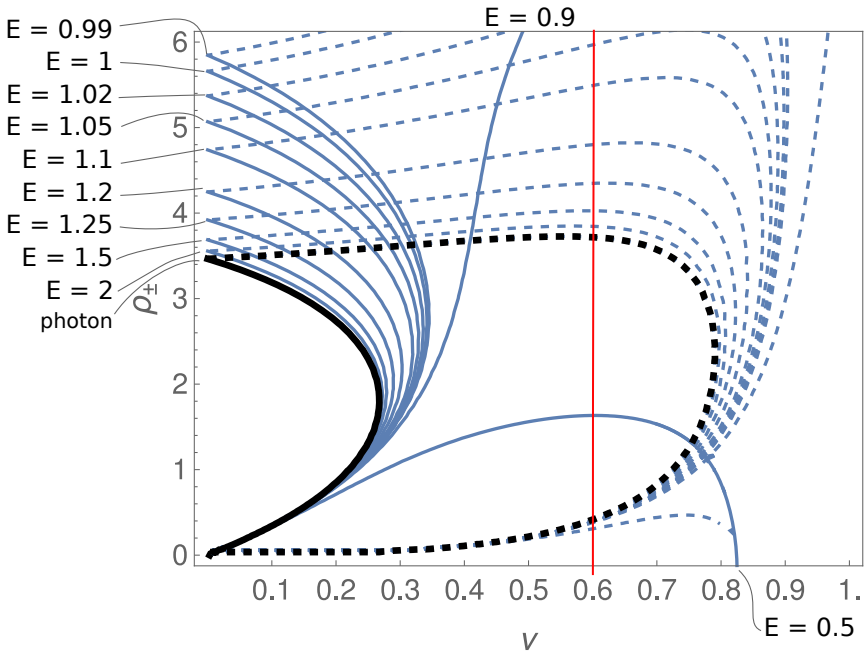

Figure 14: Merging of the bifurcation diagram of prograde (resp. retrograde) photons (shown in thick plain (resp. dashed) black line) and of a massive prograde (resp. retrograde) particle for a series of values of the energy (shown in blue plain (resp. dashed) lines). The red vertical line corresponds to looking at a spacetime with $\nu = 0.6$. The intersections of the red vertical line with the energies indicates that for the prograde massive particle, the parts of the velocity rotation curve corresponding to the lower branch will meet with the parts corresponding to the top branches without discontinuity. For the retrograde massive particle, the absence of energies allowing for a circular orbit between the two photon orbits translates to a discontinuity in the velocity rotation curve.

dotted line, corresponding to the energy of a retrograde photon on a circular orbit. Again, the intersections of the red vertical line with the lower branches of the dotted lines will correspond to the left part of the velocity rotation curve in Fig. 10, whilst its intersection with the top branches of the dotted lines will correspond to the rightmost part of the velocity rotation curve.

The stability of these orbits can be determined with Fig. 15 by looking at the corresponding orange dotted curve. The orbits smaller than the inner photon orbit ($\rho_{-,i}^{0.6}$) will be stable since the second derivative of the potential is positive; for the orbits bigger than the outer photon orbit ($\rho_{-,o}^{0.6}$), they will be unstable until the degenerate orbit at $\rho \approx 12$ where $V'' = 0$.

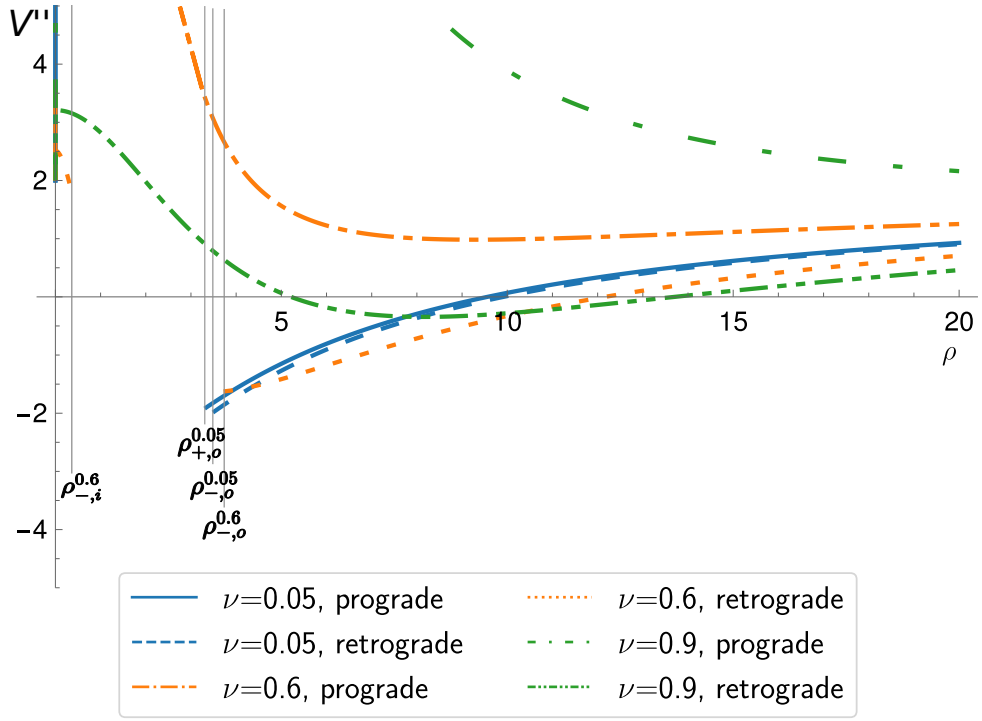

Figure 15: This graph shows the value of the second derivative for prograde and retrograde massive particles ($\mu_0 = 1$) for three different values of the NUT parameter. When $V'' > 0$ (respectively $V'' < 0$), the orbit is stable (resp. unstable). The orbits with $V'' = 0$ are degenerate.

References

[1] Manko V. S., Rodchenko E. D. and Ruiz E. 'Formation of a Kerr black hole from two stringy NUT objects'. In: *Moscow Univ. Phys.* 64 (2009), pp. 359–361. DOI: 10.3103/S0027134909040018.

[2] Clément G. 'Rotating magnetized black diholes'. In: *Physical Review D* 98.10 (Nov. 2018). ISSN: 2470-0029. DOI: 10.1103/physrevd.98.104003. URL: http://dx.doi.org/10.1103/PhysRevD.98.104003.

[3] Clément G. 'Balanced magnetized double black holes'. In: *Physics Letters B* 795 (Aug. 2019), 587–591. ISSN: 0370-2693. DOI: 10.1016/j.physletb.2019.07.008. URL: http://dx.doi.org/10.1016/j.physletb.2019.07.008.

[4] Clément G. 'The gravimagnetic dipole'. In: *Class. Quantum Grav* 38.075003 (2021). DOI: 10.1088/1361-6382/abe4ed.

[5] Takahisa I. *Deflection Angle in the Strong Deflection Limit and Quasinormal Modes in Stationary Axisymmetric Spacetimes*. 2025. arXiv: 2505.01848 [gr-qc]. URL: https://arxiv.org/abs/2505.01848.

[6] Govaerts J. 'The gravito-electromagnetic approximation to the gravimagnetic dipole and its velocity rotation curve'. In: *Classical and Quantum Gravity* 40.8 (2023), p. 085010. DOI: 10.1088/1361-6382/acc22d. URL: https://dx.doi.org/10.1088/1361-6382/acc22d.

[7] Newman E., Tamburino L. and Unti T. 'Empty-Space Generalization of the Schwarzschild Metric'. In: *Journal of Mathematical Physics* 4.7 (July 1963), pp. 915–923. ISSN: 0022-2488. DOI: 10.1063/1.1704018. URL: https://doi.org/10.1063/1.1704018.

[8] Govaerts J. *Lectures Notes in Mathematical and Theoretical Physics. Hamiltonian Quantisation and Constrained Dynamics*. Ed. by Leuven University Press. Vol. 4. B. 1991.

[9] Polchinski J. *An introduction to Bosonic String*. Ed. by Cambridge University Press. Vol. 1. String theory. 1998. DOI: 10.1017/CBO9780511816079.

[10] Beisert N. and Bröde J. *Lectures Notes from Introduction to String theory*. ETH Zürich: HS13, 2013. URL: https://people.phys.ethz.ch/~nbeisert/lectures/Strings-13HS-Notes.pdf (visited on 31/07/2024).

[11] Misner C. W., Thorne K. S. and Wheeler J. A. *Gravitation*. 1973.

[12] Landau L.D. and Lifshitz E.M. *The Classical Theory of Fields, Third Edition: Volume 2 (Course of Theoretical Physics)*. 3rd ed. Pergamon Press, 1971.